ACS Energy Letters

http://pubs.acs.org/journal/aelccp

Voltage and Temperature Limits of Advanced Electrolytes for Lithium-Metal Batteries

Isik Su Buyuker,[#] Ben Pei,[#] Hui Zhou, Xia Cao, Zhiao Yu, Sufu Liu, Weiran Zhang, Wu Xu, Ji-Guang Zhang, Zhenan Bao, Yi Cui, Chunsheng Wang, and M. Stanley Whittingham*

Cite This: *ACS Energy Lett.* 2023, 8, 1735−1743

Read Online

ABSTRACT: Several advanced electrolytes (mainly ether-based) have shown promising electrochemical performance in high-energy-density lithium-metal batteries. This work evaluates their thermal stability under abuse conditions to elucidate their safety limits compared to carbonate electrolytes typically used in Li-ion batteries. Electrolyte stability was assessed in conjunction with a $LiNi_{0.8}Mn_{0.1}Co_{0.1}O_2$ cathode and a Li-metal anode at ultra-high voltages (≤4.8 V) and temperatures (≤300 °C). The onset and extent of heat release were monitored via isothermal microcalorimetry and differential scanning calorimetry. Most ether-based electrolytes show improved thermal resilience over carbonate electrolytes. While extreme voltages severely destabilize the ether-based electrolytes, a phosphate-based localized high-concentration electrolyte exhibits improved stability over carbonate electrolytes, even at 60 °C. Although thermal analysis during the first charge process may be insufficient to conclude the long-term advantages of these electrolytes, a more stable electrolyte identified under extreme voltage and temperature conditions provides valuable guidance for the safety of future electrolyte designs.

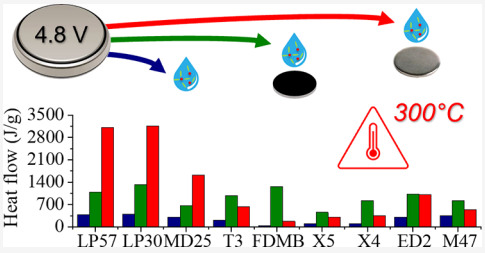

The climate crisis demands immediate decarbonization of energy production, which is stalled by the intermittent nature of renewables such as solar, wind, and hydropower. As a result, there is an ever-growing pressure to develop high-energy storage systems to store the renewable energy and level the load. In addition, to impede severe environmental deterioration caused by fossil fuel consumption, there is an urgent need to expand the electrification of the transport sector and enable wider use of renewable energy in our society. The needed expansion can only occur if high-energy storage is available. Especially in the electric vehicle field, high-energy batteries are highly demanded to provide performance comparable with that of conventional internal combustion engine vehicles and propel the expansion of electric vehicles in our society, which can largely eliminate greenhouse gas emissions from motor vehicles.

The need for higher energy density storage systems has revived the interest in lithium-metal batteries (LMBs). A Li-metal anode (LMA) has always been seen as the holy grail for batteries because it is the lightest metal that contributes to an extremely high theoretical specific capacity, 3860 mAh/g, having the lowest electrochemical potential of −3.040 V vs standard hydrogen electrode.[1] There have been many applications of LMAs in primary batteries before now.[2] Although a LMA was adopted in the groundwork of rechargeable Li batteries in the 1970s[3−5] and had been applied in the early rechargeable Li batteries in the 1970s,[6,7] the safety issues associated with dendritic Li formation and low Coulombic efficiency (CE) hindered the viability of their development and use in practice. The ever-growing demand for higher energy density batteries revived the interest in realizing viable LMBs, and the collective knowledge about this anode gained over many years of studies is hoped to be able to solve these challenges.[8] With this goal in mind, the Battery500 Consortium, launched in 2016, leads a collaborative effort to develop next-generation LMBs delivering specific energy up to 500 Wh/kg, which is more than double that of state-of-the-art Li-ion battery technologies and aims to provide electric vehicle manufacturers with more reliable batteries that are high-performing, safe, and less expensive.

The critical challenges for high-energy LMBs are the formation of dendritic Li, poor CE, and compatibility issues with high-voltage cathodes. To address these issues, one core strategy is to create novel electrolytes that can stabilize the interface to suppress Li dendrite formation and support high-voltage cathodes. Most electrolyte solvents are unstable against

Received: January 31, 2023
Accepted: March 7, 2023
Published: March 13, 2023

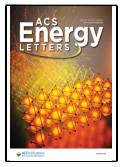

https://doi.org/10.1021/acsenergylett.3c00235
ACS Energy Lett. 2023, 8, 1735−1743

Table 1. List of Electrolytes and Their Properties[a]

Carbonate-Based Electrolytes					
Electrolyte composition	Name	Ionic conductivity (mS/cm) (25 °C)	Viscosity (cP) (25 °C)	Density (g/cm^3)	Boiling point (°C)
1 M $LiPF_6$ in EC-DMC (1:1)	LP30	~10	3.5	1.30	EC: 248[15]
1 M $LiPF_6$ in EC-EMC (3:7)	LP57	8.88	3.0	1.07	DMC: 90
1 M $LiPF_6$− 0.125 M $LiNO_3$−0.025 M $Mg(TFSI)_2$ in FEC-EMC (3:7, v/v)	MD25[16]	7.49	3.16	1.27	EMC: 110 FEC: 210

Ether-Based Electrolytes						
Electrolyte type	Electrolyte composition	Name	Ionic conductivity (mS/cm) (25 °C)	Viscosity (cP) (25 °C)	Density (g/cm^3)	Boiling point (°C)
Fluorinated	1 M LiFSI in FDMB	FDMB[13]	3.5	5	1.25	~150
	1.2 M LiFSI in F5DEE	X5[14]	5.01 ± 0.09	3.39	1.42	>170
	1.2 M LiFSI in F4DEE with 2 wt% LiDFOB	X4[14]	~4.76 ± 0.007	~6.97	~1.38	>170
LHCE	1.54 M LiFSI in DME-TTE (22:78, v/v)	M47[12]	2.44	4.92	1.48	DME: 85
	1.54 M LiFSI in DME-TFEO (21.5:78.5, v/v)	ED2[11]	1.79	6.23	1.46	TTE: 93.2 TFEO: 144
Phosphate-based LHCE	1.05 M LiFSI in TEPa-OTE (1:3, v/v)	T3	0.36	5.5	1.49	TEPa: 220 OTE: 113

[a]Abbreviations: $LiPF_6$, lithium hexafluorophosphate; EC, ethylene carbonate; DMC, dimethyl carbonate; EMC, ethyl methyl carbonate; FEC, fluoroethylene carbonate; $Mg(TFSI)_2$, magnesium bis(trifluoromethanesulfonyl)imide; $LiNO_3$, lithium nitrate; LiFSI, lithium bis(fluorosulfonyl)-imide; FDMB, fluorinated 1,4-dimethoxybutane; F5DEE, 1-(2,2-difluoroethoxy)-2-(2,2,2-trifluoroethoxy)ethane; F4DEE, 1,2-bis(2,2-difluoro-ethoxy)ethane; LiDFOB, lithium difluoro-oxalato borate; DME, 1,2-dimethoxyethane; TTE, 1,1,2,2-tetrafluoroethyl 2,2,3,3-tetrafluoropropyl ether; TFEO, tris(2,2,2-trifluoroethyl) orthoformate; TEPa, triethyl phosphate; OTE, 1*H*,1*H*,5*H*-octafluoropentyl 1,1,2,2-tetrafluoroethyl ether.

the strongly reducing Li metal at low voltages and oxidizing cathodes at high voltages. After many years of exploration, several advanced electrolytes have been developed, including localized high-concentration electrolytes (LHCEs).[9−11] LHCEs can benefit from reducing the free solvent in the Li^+ solvation structure, thereby enhancing the Li CE in high-concentration electrolytes (HCEs) while mitigating the poor wetting and conductivity of the HCE by adding functional solvent(s) as diluent in it, typically consisting of partially fluorinated ether molecules. The fluorinated ether solvent can help form a robust LiF-rich solid−electrolyte interphase (SEI), which can improve the Li CE through the Li-friendly ether backbone and shift the oxidation stability to a higher voltage via terminal C−F groups.[12−14] Triethyl phosphate is another promising solvating solvent for use in LHCEs which has been shown to alleviate the severe unfavorable side reactions and reduce the flammability of electrolytes.[10,15] To enhance the anodic stability, newly designed carbonate electrolyte formulations, made with a multi-salt strategy, have been shown to boost $LiNO_3$ dissolution in the carbonate solvent with the addition of divalent salts.[16,17] The combination of $LiNO_3$ and $LiPF_6$ in the carbonate solvents forms an inorganic-rich SEI and cathode−electrolyte interphase (CEI), enabling the Li anode to achieve a high Li CE and high-voltage NMC811 cathodes to realize a long cycle life, with the additional benefit of using salts with lower cost than pure lithium bis(fluorosulfonyl)imide (LiFSI).[18] Although these new electrolytes can outperform commercial carbonate electrolytes in LMBs electrochemically, their safety and stability windows are vastly unexplored.

In this study, the thermal stability of seven newly developed electrolytes were evaluated and compared to those of two commercial carbonate electrolytes, 1 M $LiPF_6$/EC:DMC (LP30) and 1 M $LiPF_6$/EC:EMC (LP57) (all electrolyte compositions are summarized in Table 1, including definitions of the abbreviations used). Two types of measurements were performed for the evaluations. One is differential scanning calorimetry (DSC), in which active materials and electrolytes are subjected to elevated temperatures (as high as 300 °C) to compare the thermal runaway during a dynamic heating process.[19,20] Using this method, thermal stability is tested not only for the electrolyte itself but also in coexistence with a highly charged $LiNi_{0.8}Mn_{0.1}Co_{0.1}O_2$ (NMC811) cathode (charged to 4.8 V) or a charged LMA. The other is isothermal microcalorimetry (IMC), which is employed to monitor the real-time heat evolution from full cells during a charging process, including the listed electrolytes. IMC is an operando technique that can monitor a cell's thermal evolution during electrochemical cycling. It has been extensively used to study parasitic reactions in Li-ion batteries and to understand thermal signs in cell degradation.[21−23] Real-time monitoring of the heat flow generated by all cell components and processes provides valuable insight to pinpoint the sources and extent of side reactions. The measured heat is a sum of contributions from reversible Faradaic reactions at the electrodes as well as the irreversible parasitic reactions that result in cell degradation. Identifying the onset and culmination of parasitic reactions can elucidate the limits of safe cell operation and the conditions at which cell components and the electrolyte have optimal stability. To push the limits of stability and match the DSC studies, the operando measurements were performed by charging cells to 4.8 V and at isothermal temperatures of 32 °C, 45 °C, and 60 °C to mimic the different working conditions of the cell. This preliminary study is expected to provide a rough estimation of the safety of these new electrolytes and is hoped to also

https://doi.org/10.1021/acsenergylett.3c00235
ACS Energy Lett. 2023, 8, 1735−1743

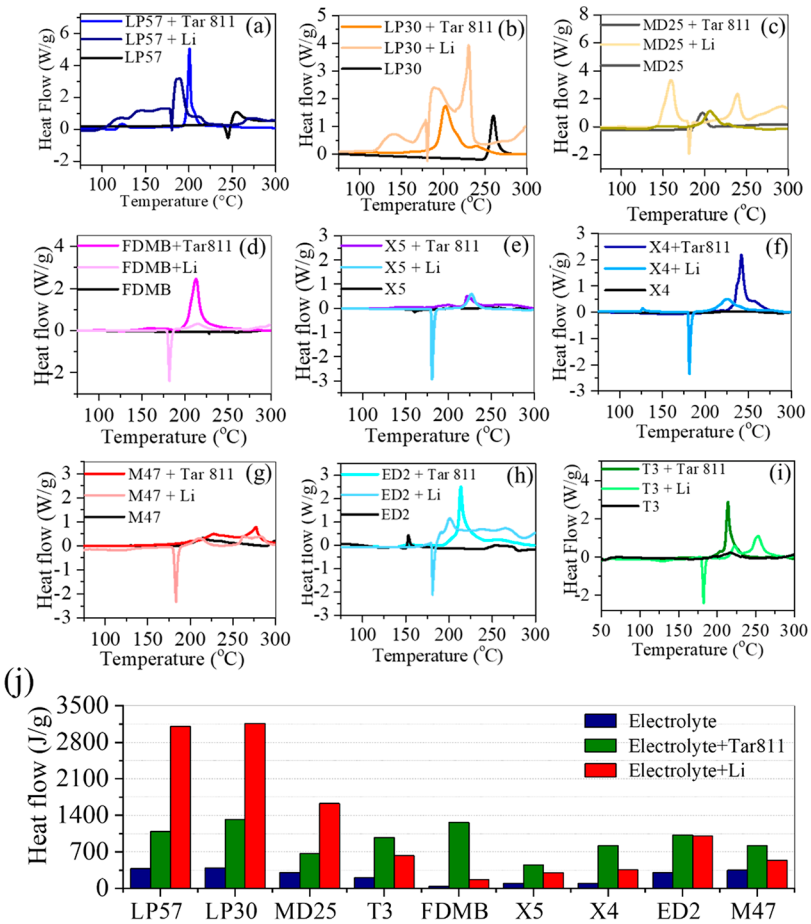

Figure 1. Ex situ DSC profiles of electrolyte only, electrolyte + Targray NMC811 charged to 4.8 V, and electrolyte + Li-metal anode after being charged with the electrolytes listed in Table 1: (a) commercial LP57, (b) commercial LP30, (c) MD25, (d) FDMB, (e) X5, (f) X4, (g) M47, (h) ED2, and (i) T3. The total integrated heat released from each experiment is summarized in (j).

provide the groundwork for the exploration of better electrolytes in the future.

Thermal Runaway Tests at Elevated Temperatures via Ex Situ Calorimetry. The high-temperature thermal stabilities of different electrolytes in conjunction with active materials were studied using DSC. To avoid interference from the ambient environment and any possible heat loss through the gas release during the tests, high-pressure capsules containing active materials and electrolyte were assembled inside a glovebox to accurately monitor any thermal decomposition as the cell components were heated to 300 °C. To pinpoint the main sources of thermal instability, electrolytes were heated not only by themselves but also in the presence of the NMC811 cathode or LMA, after the cathode and anode were charged to 4.8 V with each electrolyte. The results are summarized and compared in Figures 1 and S3. There are two critical temperatures for the measured heat flow: one is the onset temperature, indicating the starting point of exothermic heat generation, and the other is the peak temperature, marking the moment when the intense thermal runaway reaction happens. Considering electrolyte only, most ether-based electrolytes do not have the apparent exothermal peaks that are observed for carbonate-based electrolytes, although some exhibit a slightly lower onset temperature. The integrated exothermic heat flow during heating, summarized in Figure 1j (blue bars), also shows smaller heat releases for almost all ether-based electrolytes than for the carbonate-based electrolytes, indicating former have better thermal stability than the latter if considering the electrolyte only. This could be attributed to the higher thermal stability of the salt−solvent pairs used in the ether-based electrolytes. LiFSI salt is known to have better stability than $LiPF_6$, as $LiPF_6$ can catalyze chain reactions with itself as well as with the organic solvent molecules.[15] In addition, fluorinated ether and carbonate solvents can have superior thermal resilience over non-fluorinated carbonate and ether solvents.[24,31]

The thermal runaway behavior changed significantly when the charged NMC811 cathode and electrolytes were heated in conjunction. Almost every electrolyte produced an enhanced exothermic response during the heating, and both onset and peak temperatures shifted to lower values (Figure S3), indicating worse thermal stability in the presence of the charged cathode. This is likely due to the high reactivity of the Ni-rich NMC cathode (NMC811), especially at the high state of charge (SOC) (charged to 4.8 V), exacerbating the side reactions with the electrolytes and reducing the thermal stability. However, comparatively, most ether-based electrolytes still exhibited higher heat release peak temperatures (Figure S3b) and smaller integrated heat flow than the two commercial carbonate electrolytes (LP30 and LP57). This is especially notable for the recently reported fluorinated ether electrolyte X5, which showed less than half the heat release observed in LP30 (green bars in Figure 1j). The multi-salt carbonate electrolyte (MD25) also released less heat during

https://doi.org/10.1021/acsenergylett.3c00235
ACS Energy Lett. 2023, 8, 1735−1743

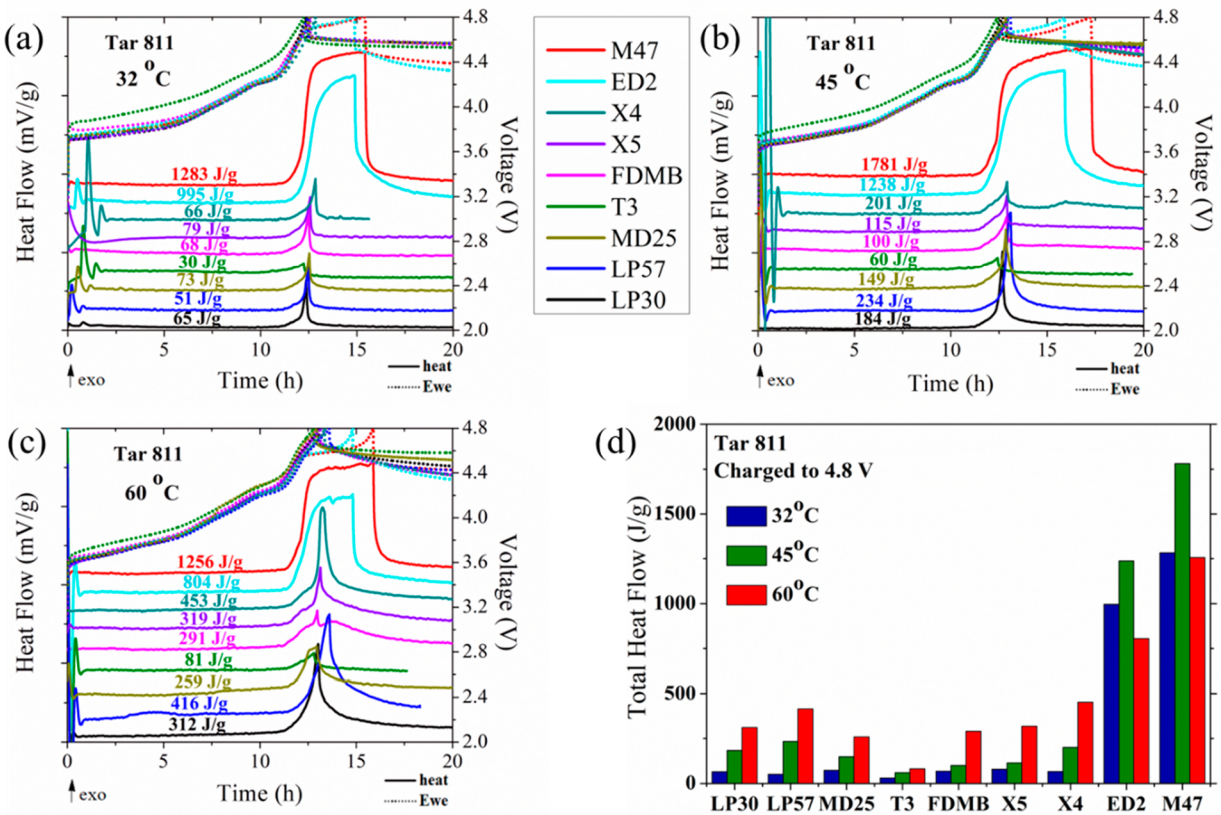

Figure 2. Heat flow measurements via isothermal microcalorimetry from Li-metal coin cells with Targray NMC811, galvanostatically charged to 4.8 V at (a) 32 °C, (b) 45 °C, and (c) 60 °C isothermally, and rested at open-circuit voltage. Dotted curves represent electrochemical profiles, and solid curves show the measured heat flow. Upward features in the heat curves indicate an exothermic response. (d) Summarized integrated heat release for different electrolytes.

the heating than the two commercial carbonate electrolytes (LP30 and LP57), although they have similar thermal behaviors for the electrolyte alone.

Ether-based electrolytes have traditionally been used with LMAs, due to the ether backbone's ability to solvate Li^+, providing a higher CE than carbonate solvents. While common ether solvents such as 1,2-dimethoxyethane (DME) are known to have low thermal stability (BP = 85 °C) and low oxidative potential (<4.0 V vs Li^+/Li), by using co-solvents/additives and higher salt concentrations, both thermal and high-voltage performance can be improved.[10,25] Utilizing high-stability salts and solvent additives can help passivate the highly reactive surface of the Ni-rich NMC cathode and LMA, thereby limiting the side reactions between the electrode surfaces and the electrolyte. Although all these new electrolytes were initially designed to stabilize the cycling of LMA, they can also function to form thin and stable CEI films on the surface of cathode particles.[25] To verify that the increased heat release with the electrolytes in the presence of the charged cathode was mainly a result of parasitic reactions between the cathode and the electrolyte, not solely due to the reactive cathode itself, the charged NMC811 powders were heated to 300 °C without any electrolyte (Figure S4). Regardless of whether charging was performed in a commercial carbonate electrolyte or a new ether-based electrolyte, the cathode powders heated by themselves all showed a similar heat release. An exotherm is observed as the temperature exceeds 190 °C, which marks the onset of thermal decomposition of the NMC811 cathode. The resultant heat flow from the cathode by itself was comparable to that of the electrolytes only and much smaller than the heat release when the cathode and electrolytes co-existed in the same capsule. Thus, the highly reactive charged cathode itself is not the main cause of the severely worse thermal stability of the cathode + electrolyte systems, verifying the major contribution to be from the side reactions between them. Furthermore, while NMC811 and carbonate electrolytes exhibit high-intensity reactions concurrent with the thermal decomposition temperature of the NMC811 cathode, the peak temperatures for the exotherms with ether electrolytes are delayed to higher temperatures, especially with fluorinated ether electrolytes X4, X5, and FDMB (Figure S3a).

The thermal behaviors at elevated temperatures were also evaluated when these electrolytes coexisted with the post-charge LMAs. As expected, both the modified carbonate-based electrolyte and the ether-based electrolytes produced significantly less heat release than the two commercialized carbonate electrolytes (LP30 and LP57) (red bars in Figure 1j), manifesting their ability to be better at stabilizing the Li-metal surface. All $LiPF_6$-containing carbonate electrolytes (LP30, LP57, MD25) showed earlier onset for exothermic reactions, below the melting point of Li-metal (180.5 °C), whereas the major exotherms with LiFSI-containing ether electrolytes and LMA appeared past the melting point of Li. Although the multi-salt carbonate electrolyte MD25 showed higher reactivity with LMA than the LiFSI-ether electrolytes, the total heat flow was less than those of LP30 and LP57. Blending Li salts is a commonly used strategy to enhance the performance and safety of electrolytes by synergistically

https://doi.org/10.1021/acsenergylett.3c00235
ACS Energy Lett. 2023, 8, 1735−1743

utilizing the desired properties of different salts. $LiNO_3$ is a salt additive commonly paired with $LiPF_6$ and LiFSI for its tendency to promote a Li_2O-rich SEI.[17,18] The MD25 electrolyte benefits from $LiNO_3$ salt additive, as well as the fluorinated fluoroethylene carbonate (FEC) co-solvent, which is another passivating additive that promotes the desired inorganic SEI, thereby showing improved stability with LMA over the LP30 and LP57 electrolytes.[15] On the other hand, concentrated LiFSI has been shown to have better stability with LMA than $LiPF_6$ even in the carbonate solvents ethylene carbonate (EC) and dimethyl carbonate (DMC).[26] This is typically attributed to the high reactivity of FSI^- with the LMA, forming a LiF-rich SEI.[10,27] Such SEIs formed in the electrolytes beyond LP57 and LP30 are rich in inorganic species (LiF, Li_xO, or Li_3N) compared to the SEIs formed in LP57 and LP30[10,31] and, therefore, provide better protection from thermal reactions between the LMA and the electrolyte. Furthermore, the desired LiF-rich CEIs were also found in the LHCEs (M47 and ED2) with FDMB, X5, and X4.[11−14] As a result, the reactivity of NMC811 and the electrolyte is also reduced in comparison to those of LP57 and LP30.

In conclusion, the commercial carbonate electrolytes LP30 and LP57 showed a significantly higher heat release (almost 10-fold that for electrolyte only) when heated with Li-metal, whereas the new electrolytes effectively improved their high-temperature stability with LMA to various degrees. This further verifies the poor compatibility of commercial carbonate electrolytes with LMAs, signifying the importance of exploring new electrolyte chemistries to realize viable LMBs.

Real-Time Thermal Monitoring at Extreme Voltages via Isothermal Microcalorimetry. Ex situ DSC is a valuable tool to assess the component-level thermal stability of active materials and electrolytes during a dynamic heating process. However, considering the real applications, this method is insufficient to elucidate the cell-level reactivity under harsh operating conditions such as elevated potentials and temperatures. To explore the dynamic thermal behavior of the electrolytes in coin-cell batteries including an NMC811 cathode and LMA and observe the severity of exothermic reactions, IMC was employed. The real-time heat flows from the cells were monitored while charging to extreme voltages (up to 4.8 V) at increasing isothermal temperatures (32 °C, 45 °C, and 60 °C) to evaluate the upper limit of stability and severity of heat release under these abuse conditions.

The dynamic heat flow signals and corresponding galvanic profiles were collected by using an isothermal microcalorimeter and an electrochemical cycler, and the combined results are shown in Figure 2. The exothermic events shown in the heat curves are mirrored by the features in the voltage profiles, aside from the waving peaks of heat flow signals that appeared before 2 h, which are attributed to the temperature balance of the calorimeter. All electrolytes exhibit baseline heat flow until approximately 4.4 V, even at 60 °C, after which an exothermic uptick is observed, marking the onset of exothermic side reactions. While for most electrolytes this exothermic reaction exhibits a single peak or bump, the LHCEs present a distinct plateau-like feature in both voltage and heat flow curves. The two LHCEs, M47 and ED2, similarly formulated with LiFSI and DME, suffer from an extended side reaction as the potential exceeds typical operating limits (>4.4 V), where a significantly higher exothermic heat flow is prompted. This could be due to the high-voltage instability of the non-fluorinated ether solvent DME present in both electrolytes. The 1 M LiFSI/DME electrolyte is known to have a low oxidative stability, limited to <4 V.[13] For M47, the high-voltage exotherm is even more intense than that for ED2, the former additionally including 1,1,2,2-tetrafluoroethyl 2,2,3,3-tetrafluoropropyl ether (TTE) as a diluent instead of the tris(2,2,2-trifluoroethyl) orthoformate (TFEO) in ED2. Similar phenomena have also been observed in other ether electrolytes, like poly(ethylene glycol) (PEG), in which the ether chain (−C−O−C−) will be oxidized when the voltage is higher than 4.3 V in Li/NMC622 batteries.[28] Thus, the notable exothermic side reactions and the distinct plateau-like voltage profile above 4.5 V indicate that there may be potential safety risks under voltage abuse conditions with M47 and ED2. Once the upper voltage limit is exceeded, stability becomes compromised, prompting severe self-decomposition and cross-over parasitic reactions with other components, resulting in much higher heat generation than with other electrolytes. This speculation was further verified by another similar operando thermal measurement for M47 electrolyte with a 4.4 V cutoff voltage at 60 °C, where the heat release was significantly reduced and no plateau-like feature in either the heat flow curve or the voltage curve was observed (1256 J/g vs 46 J/g) (Figure S6).

Figure 2d summarizes the total integrated heat flow values for each electrolyte. The electrolytes based on fluorinated ether electrolytes, FDMB, X5, and X4, show high-voltage thermal stability similar to that of the commercial carbonate electrolytes LP30 and LP57 and significantly better stability compared to the DME-containing LHCEs. The improved oxidative stability of the fluorinated ether electrolytes over that of the DME-based electrolytes is likely owed to their having lower highest occupied molecular orbital levels due to the functionalized $-CF_2-$ incorporation.[13] FDMB, X5, and X4 have superior high-voltage stability up to 45 °C, after which parasitic reactions increase by nearly 3-fold. A shoulder-like exotherm emerges at 60 °C, indicating worsened side reactions at the higher temperature.

Non-flammable, phosphate-added, fluorinated ether T3 electrolyte exhibits the lowest heat flow among the tested electrolytes, indicating the highest resilience to the severe charging voltage of 4.8 V and high temperature of 60 °C. Under such abuse conditions, salts and organic solvents in the electrolyte can decompose to form radical species with high reactivity. Phosphate esters such as triethyl phosphate (TEPa) are thought to have a free-radical scavenging ability which can combat the chain-like electrolyte decomposition reactions. T3 electrolyte benefits from two flame-retardant solvents, TEPa and 1*H*,1*H*,5*H*-octafluoropentyl 1,1,2,2-tetrafluoroethyl ether (OTE).[24,29] However, TEPa does not form a stable SEI/CEI, which may reflect negatively on its electrochemical performance.[24] Thus, the use of high-boiling-point, non-flammable solvent additives can be a viable strategy to enhance the high-temperature and high-voltage resilience of electrolytes.

Similar to the results of the DSC experiments, the MD25 multi-salt carbonate electrolyte shows somewhat improved stability over the commercial carbonates, especially at elevated temperatures of 45 °C and 60 °C. The incorporation of a $LiNO_3$ salt additive and FEC co-solvent improves the high-voltage and high-temperature stability of the conventional $LiPF_6$-EC solvent pair. Typically, the exothermic flow is expected to increase when the cell temperature is increased, as elevated temperatures can prompt higher reactivity of cell materials. While this phenomenon is observed for most

https://doi.org/10.1021/acsenergylett.3c00235
ACS Energy Lett. 2023, 8, 1735−1743

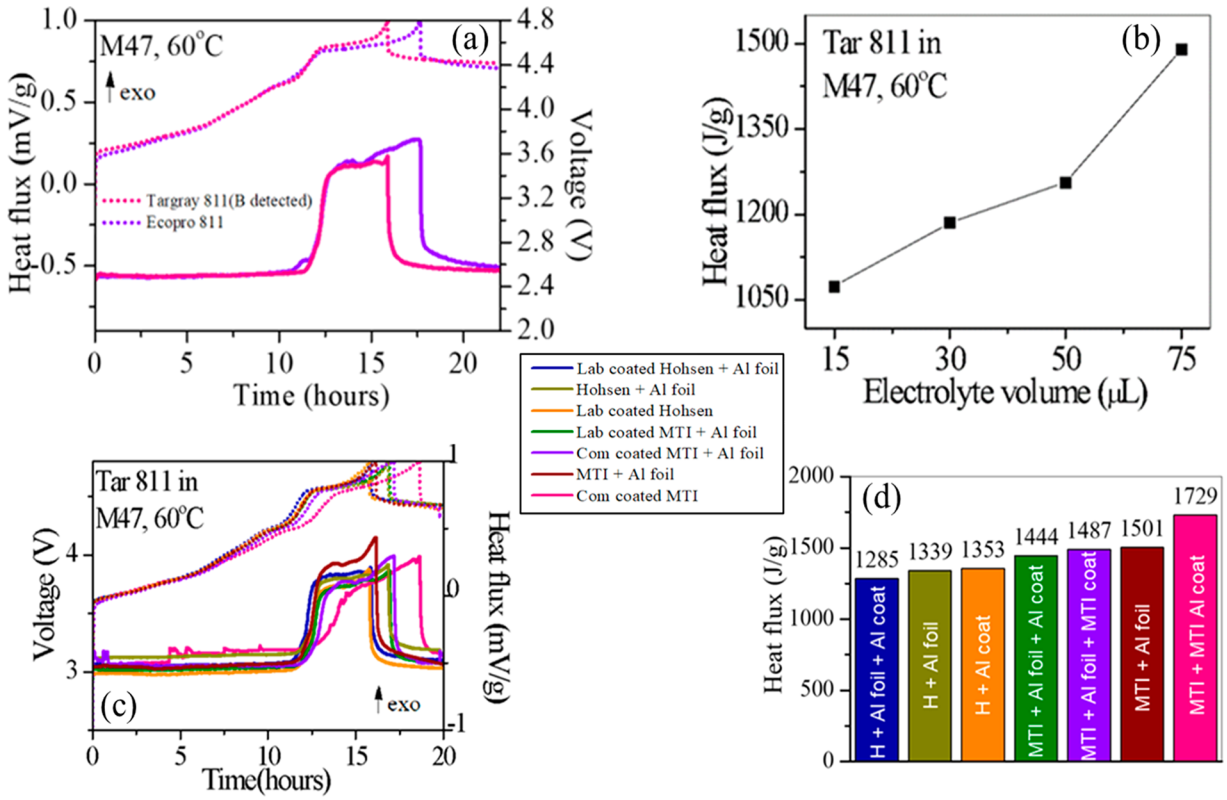

Figure 3. Operando DSC measurements performed on (a) Targray NMC811 vs EcoPro NMC811 with M47 electrolyte that were charged and rested at 4.8 V at 60 °C isothermally. Upward features in the heat curves indicate an exothermic response. Same measurements performed on Targray NMC811 with (b) different volumes of M47 electrolyte and (c) different coin cell configurations. (d) Summary of the integrated heat release for (c).

electrolytes, where temperature and heat flow present as a linear correlation, the M47 and ED2 show a different trend. For the two LiFSI-DME-containing LHCEs, the highest heat flow is observed at 45 °C, and the high-voltage plateau seems shortened at 60 °C, which can be observed more closely in Figure S7. Uncovering the reason behind this phenomenon requires further in-depth analysis, which is beyond the scope of this study.

Influence of Other Components on the Cell Thermal Stability. The above IMC measurements were carried out on Hohsen 2032-type coin cells, each containing a Targray NMC811 cathode, 50 μL of electrolyte, and 600 μm thick Li-metal anode. In a systematic study, using M47 as the sample electrolyte, it was found that when some of the cell components were changed, the heat release would be different. In Figure 3, changes in (a) cathode material (Targray or Ecopro NMC811), (b) quantity of electrolyte, and (c) coin cell parts were studied to elucidate their influence on electrolyte reactivity. The X-ray photoelectron spectroscopy (XPS) analysis of Targray NMC811 powders (Figure S8) suggests the presence of a boron-containing surface modification, although this information was not released by the vendor. Upon subjecting the two NMC811 analogues to the 4.8 V charge experiment, using an Ecopro NMC811 cathode, without any detectable coating/substitution (Figure S8), a higher heat release was observed compared to Targray NMC811, containing boron on the surface (1487 J/g vs 1256 J/g) (Figure 3a). Thus, cathode modification is a viable way to improve the thermal stability, as similarly shown in our recent work on niobium-coated/substituted NMC811.[30] This also signifies the importance of characterizing purchased materials.

Another strategy to limit cell reactivity is to reduce the amount of electrolyte in the coin cell, which can limit the extent of side reactions (Figure 3b). Although excess electrolyte is beneficial for longer cycle life as a countermeasure to electrolyte depletion, the thermal stability and the energy density of the cell may be sacrificed. Therefore, a trade-off may exist between stability and performance. LiFSI-based electrolytes are prone to corrode stainless steel coin cell parts, and it is important to reinforce the cell parts with protective coatings to reduce corrosive reactions during electrochemical testing. Figure 3c,d shows the operando DSC tests with different cell configurations (different coin cell parts, Al coating, with/without adding Al foil). The results show that, when other conditions are identical, the Hohsen coin cell produced significantly less exothermic heat in comparison to the MTI coin cell, which can be attributed to the better corrosive resistance for the former (coin cell: Hohsen SS 316L vs MTI SS304, see Figure S9). Thus, corrosive resistance properties of the coin cell parts can suppress the exothermic side reactions. Furthermore, Al protections (Al coating and Al foil addition) are a very effective strategy to impede the corrosive reactions between the electrolyte and stainless steel. These findings are a reminder that enhancing the performance of LMBs in real applications is a complex project, not only demanding optimization on the materials level but also requiring compatibility in the whole system.

The thermal stabilities of many newly developed, competitive electrolytes for LMBs were studied by ex situ DSC and

https://doi.org/10.1021/acsenergylett.3c00235
ACS Energy Lett. 2023, 8, 1735−1743

operando DSC (IMC) and compared to those of two commercial carbonate electrolytes, LP30 and LP57. For the ex situ thermal measurements at elevated temperatures up to 300 °C, the new electrolytes showed apparent advantages on suppressing the heat generation with cell active materials. This can be attributed to their specialized formulations which help stabilize the interphases either on the cathode or on the Li anode, as the parasitic reactions between the electrolyte and the cathode or anode are the main cause of severe exothermic reactions. Comparatively, the thermal behaviors of these new electrolytes during the operando measurements are mostly just slightly better or comparable to those of the two commercial carbonate electrolytes, and some are even worse, as the extreme charge voltage (4.8 V) adopted for the IMC measurements severely exceeds the safe working window for some new electrolytes. Furthermore, monitoring the heat release during the first charging process may be too constricted to determine the realistic stability of the electrolytes. Operando thermal studies with lower charge voltage and longer cycling are worthwhile to explore in the future. In addition, through studying the influence of the cell components on thermal behavior, some stabilizing strategies were identified, such as modifying the cathode materials with coating/substitution, reducing the electrolyte amount, and preventing the corrosive reactions with inactive cell components. Our studies indicate that there may be a trade-off between the quality of Li plating and the stability and lifetime of the cells.

■ METHODOLOGY

Electrode Preparation. Due to the high surface sensitivity of NMC811, all the electrode preparations were performed in a dry room (relative humidity <0.5%) to minimize exposure to moisture. Commercial NMC811 (Targray) powder was mixed with acetylene black (Alfa Aesar, 100% compressed, >99.9%) and poly(vinylidene fluoride) (PVDF) binder in a weight ratio of 90:5:5 with 1-methyl-2-pyrrolidinone (NMP) solvent (solid content is ∼45%) through a mixer (THINKY ARE 310) at the speed of 2000 rpm to fabricate the electrode slurry. The formed homogeneous slurry was cast on aluminum foil with the Comma Coating Machine (MediaTech, South Korea) inside the dry room, with a mass loading of the active material around 17−18 mg/cm^2. Then the coated electrodes were punched and calendered to 3.0 g/cm^3. For the calendering density calculations, all the solid materials on the Al current collector were considered, including active material (NMC811), PVDF binder, and carbon black. Finally, the calendered electrodes were further vacuum-dried at 120 °C for at least 2 h before they were transferred to an argon-filled glovebox for coin cell assembly.

Coin Cell Making. The 2032-type coin cells (Hohsen, Japan or MTI) were assembled for the electrochemical measurements with Li foil (600 μm) as a counter/reference electrode. A polyethylene (PE) separator (Mediatech) and 50 μL of different electrolytes (listed in Table 1) were used for cell assembly. To avoid corrosive reactions between solvents and coin cell parts, the positive coin cell caps were Al-coated and/or an additional piece of Al foil disc (12 μm thickness, 19 mm diameter) was added inside the positive cap. Assembled cells were rested at open-circuit voltage (OCV) for 24 h before electrochemical measurements.

Ex Situ Calorimetry. Ex situ experiments were performed with a TA Q200 differential scanning calorimeter by heating the sample and reference capsules from 50 °C to 300 °C at a ramping rate of 2.5 °C/min. The reference capsule contained the high-pressure (100 bar) stainless-steel pan/cover and a gold seal, and the sample capsules mirrored the contents in the reference capsule with the addition of fresh electrolyte (3 g/Ah of capacity at 4.8 V, corresponding to 5−7 μL depending on electrolyte density) and/or 10 mg of charged cathode (corresponds to 11.1 mg of cathode powder scratched off the washed cathode) and/or 5 mg of washed Li anode (including some SEI) obtained from the charged cell. The cells used in ex situ calorimetry were charged to 4.8 V at room temperature and then disassembled in an argon-filled glovebox to collect the LMA and NMC811 cathode, which were thoroughly washed with dimethyl carbonate (DMC) solvent and dried before the measurements. To compare the total heat release during the heating for different samples, the thermal curve was normally integrated from 125 °C to 300 °C (see Figure S1).

Isothermal Microcalorimetry. The IMC experiments, also denoted as operando DSC, were performed using an MMC 274 Nexus multi-module calorimeter with a high-temperature coin cell module (Netzsch), which was coupled with EC-Lab for electrochemical measurements. The coin cell module is a differential calorimeter, where the heat flow signal is the difference between the reference and sample cell outputs. The sample cells were standard assembled 2032 coin cells as described in the above Coin Cell Making section, and the reference cell was assembled the same, excluding the NMC811 cathode, LMA, and electrolyte. In the voltage abuse experiments, the sample cells were charged to 4.8 V at C/10 (1C = 200 mAh/g) inside the calorimeter at an isothermal temperature of 32 °C, 45 °C, or 60 °C. Upon reaching 4.8 V, the current was removed, and the cell was rested to establish a baseline. The total heat was obtained by integrating under the heat curves using a linear line drawn between two flat regions (baseline heat) before and after the exotherm (see Figure S2).

■ ASSOCIATED CONTENT

Supporting Information

The Supporting Information is available free of charge at https://pubs.acs.org/doi/10.1021/acsenergylett.3c00235.

Heat flow integration methods, DSC thermograms in higher visibility, supporting IMC experiments, and XPS analyses of the Targray and EcoPro NMC811 cathodes and the Hohsen and MTI coin cell parts (PDF)

■ AUTHOR INFORMATION

Corresponding Author

M. Stanley Whittingham − *Department of Chemistry, State University of New York at Binghamton, Binghamton, New York 13902, United States;* orcid.org/0000-0002-5039-9334; Email: stanwhit@gmail.com

Authors

Isik Su Buyuker − *Department of Chemistry, State University of New York at Binghamton, Binghamton, New York 13902, United States;* orcid.org/0000-0001-9058-8351

Ben Pei − *Department of Chemistry, State University of New York at Binghamton, Binghamton, New York 13902, United States*

Hui Zhou − *Department of Chemistry, State University of New York at Binghamton, Binghamton, New York 13902, United States*

https://doi.org/10.1021/acsenergylett.3c00235
ACS Energy Lett. 2023, 8, 1735−1743

Xia Cao − *Energy and Environment Directorate, Pacific Northwest National Laboratory, Richland, Washington 99354, United States;* orcid.org/0000-0003-1610-4341

Zhiao Yu − *Department of Chemical Engineering, Stanford University, Stanford, California 94305, United States;* orcid.org/0000-0001-8746-1640

Sufu Liu − *Department of Chemical and Biomolecular Engineering, University of Maryland, College Park, Maryland 20740, United States*

Weiran Zhang − *Department of Chemical and Biomolecular Engineering, University of Maryland, College Park, Maryland 20740, United States*

Wu Xu − *Energy and Environment Directorate, Pacific Northwest National Laboratory, Richland, Washington 99354, United States;* orcid.org/0000-0002-2685-8684

Ji-Guang Zhang − *Energy and Environment Directorate, Pacific Northwest National Laboratory, Richland, Washington 99354, United States;* orcid.org/0000-0001-7343-4609

Zhenan Bao − *Department of Chemical Engineering, Stanford University, Stanford, California 94305, United States;* orcid.org/0000-0002-0972-1715

Yi Cui − *SLAC National Accelerator Laboratory, Stanford Institute for Materials and Energy Sciences, Menlo Park, California 94025, United States;* orcid.org/0000-0002-6103-6352

Chunsheng Wang − *Department of Chemical and Biomolecular Engineering, University of Maryland, College Park, Maryland 20740, United States;* orcid.org/0000-0002-8626-6381

Complete contact information is available at: https://pubs.acs.org/10.1021/acsenergylett.3c00235

Author Contributions

[#]I.S.B. and B.P contributed equally to this work.

Notes

The authors declare no competing financial interest.

■ ACKNOWLEDGMENTS

This work was supported by the Assistant Secretary for Energy Efficiency and Renewable Energy, Office of Vehicle Technologies of the U.S. Department of Energy, through the Advanced Battery Materials Research Program (Battery500 Consortium), award no. DEEE0007765.

■ REFERENCES

(1) Lewis, G. N.; Keyes, F. G. The Potential of the Lithium Electrode. *J. Am. Chem. Soc.* **1913**, *35* (4), 340−344.

(2) Meyers, W. F.; Simmons, J. W. Electric Current-Producing Cell with Anhydrous Organic Liquid Electrolyte. U.S. Patent US3423242A, 1969.

(3) Whittingham, M. S. Batterie à Base de Chalcogénures. Belgian Patent BE819672A, 1975.

(4) Whittingham, M. S. Electrical Energy Storage and Intercalation Chemistry. *Science* **1976**, *192* (4244), 1126−1127.

(5) Whittingham, M. S. Chalcogenide Battery. U.S. Patent US4009052A, 1977.

(6) Akridge, J. R.; Vourlis, H. Performance of Li/TiS2 solid state batteries using phosphorous chalcogenide network former glasses as solid electrolyte. *Solid State Ionics* **1988**, *28*−*30*, 841−846.

(7) Abraham, K. M.; Pasquariello, D. M.; Schwartz, D. A. Practical rechargeable lithium batteries. *J. Power Sources* **1989**, *26* (1), 247−255.

(8) Lin, D.; Liu, Y.; Cui, Y. Reviving the lithium metal anode for high-energy batteries. *Nat. Nanotechnol* **2017**, *12* (3), 194−206.

(9) Cao, X.; Ren, X.; Zou, L.; Engelhard, M. H.; Huang, W.; Wang, H.; Matthews, B. E.; Lee, H.; Niu, C.; Arey, B. W.; et al. Monolithic solid−electrolyte interphases formed in fluorinated orthoformate-based electrolytes minimize Li depletion and pulverization. *Nature Energy* **2019**, *4* (9), 796−805.

(10) Cao, X.; Jia, H.; Xu, W.; Zhang, J.-G. Review—Localized High-Concentration Electrolytes for Lithium Batteries. *J. Electrochem. Soc.* **2021**, *168* (1), 010522.

(11) Cao, X.; Gao, P.; Ren, X.; Zou, L.; Engelhard, M. H.; Matthews, B. E.; Hu, J.; Niu, C.; Liu, D.; Arey, B. W.; et al. Effects of fluorinated solvents on electrolyte solvation structures and electrode/electrolyte interphases for lithium metal batteries. *Proc. Natl. Acad. Sci. U. S. A.* **2021**, *118* (9), No. e2020357118.

(12) Ren, X.; Zou, L.; Cao, X.; Engelhard, M. H.; Liu, W.; Burton, S. D.; Lee, H.; Niu, C.; Matthews, B. E.; Zhu, Z.; et al. Enabling High-Voltage Lithium-Metal Batteries under Practical Conditions. *Joule* **2019**, *3* (7), 1662−1676.

(13) Yu, Z.; Wang, H.; Kong, X.; Huang, W.; Tsao, Y.; Mackanic, D. G.; Wang, K.; Wang, X.; Huang, W.; Choudhury, S.; et al. Molecular design for electrolyte solvents enabling energy-dense and long-cycling lithium metal batteries. *Nature Energy* **2020**, *5* (7), 526−533.

(14) Yu, Z.; Rudnicki, P. E.; Zhang, Z.; Huang, Z.; Celik, H.; Oyakhire, S. T.; Chen, Y.; Kong, X.; Kim, S. C.; Xiao, X.; et al. Rational solvent molecule tuning for high-performance lithium metal battery electrolytes. *Nature Energy* **2022**, *7* (1), 94−106.

(15) Luo, D.; Li, M.; Zheng, Y.; Ma, Q.; Gao, R.; Zhang, Z.; Dou, H.; Wen, G.; Shui, L.; Yu, A.; et al. Electrolyte Design for Lithium Metal Anode-Based Batteries Toward Extreme Temperature Application. *Adv. Sci. (Weinh)* **2021**, *8* (18), No. e2101051.

(16) Liu, S.; Xia, J.; Zhang, W.; Wan, H.; Zhang, J.; Xu, J.; Rao, J.; Deng, T.; Hou, S.; Nan, B.; et al. Salt-in-Salt Reinforced Carbonate Electrolyte for Li Metal Batteries. *Angew. Chem., Int. Ed.* **2022**, *61* (43), No. e202210522.

(17) Liu, S.; Ji, X.; Piao, N.; Chen, J.; Eidson, N.; Xu, J.; Wang, P.; Chen, L.; Zhang, J.; Deng, T.; et al. An Inorganic-Rich Solid Electrolyte Interphase for Advanced Lithium-Metal Batteries in Carbonate Electrolytes. *Angew. Chem., Int. Ed. Engl.* **2021**, *60* (7), 3661−3671.

(18) Xu, G.; Shangguan, X.; Dong, S.; Zhou, X.; Cui, G. Formulation of Blended-Lithium-Salt Electrolytes for Lithium Batteries. *Angew. Chem., Int. Ed. Engl.* **2020**, *59* (9), 3400−3415.

(19) Li, Z.; Chernova, N. A.; Feng, J.; Upreti, S.; Omenya, F.; Whittingham, M. S. Stability and Rate Capability of Al Substituted Lithium-Rich High-Manganese Content Oxide Materials for Li-Ion Batteries. *J. Electrochem. Soc.* **2011**, *159* (2), A116.

(20) Huang, Y.; Lin, Y.-C.; Jenkins, D. M.; Chernova, N. A.; Chung, Y.; Radhakrishnan, B.; Chu, I.-H.; Fang, J.; Wang, Q.; Omenya, F.; et al. Thermal Stability and Reactivity of Cathode Materials for Li-Ion Batteries. *ACS Appl. Mater. Interfaces* **2016**, *8* (11), 7013−7021.

(21) Glazier, S. L.; Li, J.; Louli, A. J.; Allen, J. P.; Dahn, J. R. An Analysis of Artificial and Natural Graphite in Lithium Ion Pouch Cells Using Ultra-High Precision Coulometry, Isothermal Microcalorimetry, Gas Evolution, Long Term Cycling and Pressure Measurements. *J. Electrochem. Soc.* **2017**, *164* (14), A3545.

(22) Huie, M. M.; Bock, D. C.; Wang, L.; Marschilok, A. C.; Takeuchi, K. J.; Takeuchi, E. S. Lithiation of Magnetite (Fe3O4): Analysis Using Isothermal Microcalorimetry and Operando X-ray Absorption Spectroscopy. *J. Phys. Chem. C* **2018**, *122* (19), 10316−10326.

(23) Faenza, N. V.; Lebens-Higgins, Z. W.; Mukherjee, P.; Sallis, S.; Pereira, N.; Badway, F.; Halajko, A.; Ceder, G.; Cosandey, F.; Piper, L. F. J.; et al. Electrolyte-Induced Surface Transformation and Transition-Metal Dissolution of Fully Delithiated LiNi0.8Co0.15Al0.05O2. *Langmuir* **2017**, *33* (37), 9333−9353.

(24) Zhang, Q.-K.; Zhang, X.-Q.; Yuan, H.; Huang, J.-Q. Thermally Stable and Nonflammable Electrolytes for Lithium Metal Batteries: Progress and Perspectives. *Small Science* **2021**, *1* (10), 2100058.

(25) Ren, X.; Gao, P.; Zou, L.; Jiao, S.; Cao, X.; Zhang, X.; Jia, H.; Engelhard, M. H.; Matthews, B. E.; Wu, H.; et al. Role of inner solvation sheath within salt−solvent complexes in tailoring electrode/electrolyte interphases for lithium metal batteries. *Proc. Natl. Acad. Sci. U. S. A.* **2020**, *117* (46), 28603−28613.
(26) Peng, Y.; Nishikawa, K.; Kanamura, K. Effects of Carbonate Solvents and Lithium Salts in High-Concentration Electrolytes on Lithium Anode. *J. Electrochem. Soc.* **2022**, *169* (6), 060548.
(27) Miao, R.; Yang, J.; Feng, X.; Jia, H.; Wang, J.; Nuli, Y. Novel dual-salts electrolyte solution for dendrite-free lithium-metal based rechargeable batteries with high cycle reversibility. *J. Power Sources* **2014**, *271*, 291−297.
(28) Yang, X.; Jiang, M.; Gao, X.; Bao, D.; Sun, Q.; Holmes, N.; Duan, H.; Mukherjee, S.; Adair, K.; Zhao, C.; et al. Determining the limiting factor of the electrochemical stability window for PEO-based solid polymer electrolytes: main chain or terminal −OH group? *Energy Environ. Sci.* **2020**, *13* (5), 1318−1325.
(29) Zheng, J.; Ji, G.; Fan, X.; Chen, J.; Li, Q.; Wang, H.; Yang, Y.; DeMella, K. C.; Raghavan, S. R.; Wang, C. High-Fluorinated Electrolytes for Li−S Batteries. *Adv. Energy Mater.* **2019**, *9* (16), 1803774.
(30) Xin, F.; Zhou, H.; Zong, Y.; Zuba, M.; Chen, Y.; Chernova, N. A.; Bai, J.; Pei, B.; Goel, A.; Rana, J.; et al. What is the Role of Nb in Nickel-Rich Layered Oxide Cathodes for Lithium-Ion Batteries? *ACS Energy Letters* **2021**, *6* (4), 1377−1382.
(31) Cheng, X. B.; Zhang, R.; Zhao, C. Z.; Zhang, Q. Toward Safe Lithium Metal Anode in Rechargeable Batteries: A Review. *Chem. Rev.* **2017**, *117* (15), 10403−10473.

https://doi.org/10.1021/acsenergylett.3c00235
ACS Energy Lett. 2023, 8, 1735−1743